Available online at www.sciencedirect.com
SCIENCE DIRECT
Polymer 46 (2005) 7684–7694
polymer
www.elsevier.com/locate/polymer

Numerical simulation of substrate effects on spinodal decomposition in polymer binary mixture: morphology and dynamics

Li-Tang Yan, Xu-Ming Xie*

Advanced Materials Laboratory, Department of Chemical Engineering, Tsinghua University, Beijing 100084, People's Republic of China

Received 29 January 2005; received in revised form 17 May 2005; accepted 28 May 2005
Available online 6 July 2005

Abstract

The characteristic features of the morphology and dynamics of binary mixture for substrate-directed spinodal decomposition (SDSD) in three dimensions have been studied using numerical simulations. The simulation results show that the formation of the wetting layer on the substrate interface follows the power-law growth. It is found that the continuous influence of anisotropic diffusive behavior arose by wetting of substrate induces the wetting component spreading onto the interface of the substrate randomly. The phase morphology and averaged size in the vicinity of the substrate fluctuate greatly due to the wetting of the substrate. The self-similar evolution of the cross-sections parallel and perpendicular to the substrate interface is discussed by relevant scale law functions, respectively. And the mechanisms of the growth in both the parallel and perpendicular directions are also investigated.

Keywords: Substrate effect spinodal decomposition; Cell dynamic system; Simulation

1. Introduction

In recent years, much attention has been paid to the phase separation morphology and dynamics of binary (AB) mixture in the presence of substrate with a preferential wetting for one component of the mixture [1–10]. It has been recognized that, in the vicinity of substrate, the process of spinodal decomposition may be severely changed compared to that of bulk [11]. Typically, the substrate interface is completely or partially wetted by the preferred component and becomes the origin of anisotropic spinodal decomposition waves, which propagates into the bulk perpendicular to the surface. This phenomenon has been referred to as 'surface-directed spinodal decomposition' [1–3].

To our knowledge, the first relevant experimental study of this problem owes to Jones et al. [3] who found an oscillatory composition profile near the substrate of anisotropic polymer mixture after a quench into the two-phase region. Krausch et al. [4] and Straub et al. [12] found that the preferred phase initially formed a plated cross-section on the substrate. Wiltzius, Cumming and their co-workers [13,14] observed that the structure factor of the coarsening system exhibited two peaks and, the position of the first peak (at small wave number) exhibited an abnormal fast growth law, i.e. $L_1(t) \propto t^{\Theta}$ with $\Theta \approx 1.1$. However, in contrast to the above experiments, Guenoun et al. [15] and others [5,15–17] found that the phase growth parallel to the substrate surface was suppressed and, if a power law fit was attempted, it would show a crossover of the exponent from 1/3 to 1/2. It is even greater interest to study the opposite limit of a strong surface field [18,19]. In this case, there is rapid formation of a multi-cross-sectioned structure at the surface. Recent interest has also focused on SDSD in other contexts, such as SDSD on patterned substrates [20,21], spinodal dewetting [22,23] and so on.

Along with the experimental observation, computer simulation is playing an increasingly important role in understanding the mechanism of morphology changes in binary mixture [24–39]. The SDSD of binary mixture has also been extensively investigated by Langevin simulation [27–31], cell dynamic system (CDS) [32,33], microscopic models (e.g. the spin-exchange Ising model) [34,35] and Monte Carlo simulation [36]. These modeling have also been extended naturally to the problem of phase separation

* Corresponding author. Tel.: +86 10 6277 36073.
E-mail address: xxm-dce@mail.tsinghua.edu.cn (X.-M. Xie).

0032-3861/$ - see front matter © 2005 Elsevier Ltd. All rights reserved.
doi:10.1016/j.polymer.2005.05.115

in a confined geometry (e.g. thin film), where novel physical effects arise due to the interplay for SDSD waves arising from different boundaries. For example, Puri, Binder, and Frisch [27,28] formulated phenomena models, which are δ-function [27] for short-range potential and power-law [28] for long-range potential on the preferred component, respectively, based on the Cahn–Hilliard (CH) equation. They have studied domain growth adjacent to the wetting layer for both a critical quench [27,28] and an off-critical quench [29,30] with a variety of surface potentials. Binder and Frisch [34] applied a master equation deduced by the Ising model with Kawasaki spin-exchange kinetics to the semi-infinite Ising model with a δ-function surface field and Kawasaki kinetics. Marko [32] also considered SDSD in 2D with both short-range and long-range surface forces by CDS. Employing Monte Carlo simulation, Rysz [36] studied the SDSD in thin polymer blend film.

So far most previous simulations have been limited to two dimensions. And almost all the previous study, even a few works in 3D focused on the cross-section perpendicular to the substrate surface. The phase evolution of the cross-section parallel to the substrate was only characterized using the characteristic length obtained from laterally averaged correlation function. In this case, the morphology and dynamics of the cross-section parallel to substrate surface were almost omitted. However, these simulations could not give an overall view about the dynamics of the phase evolution in SDSD. As a matter of fact, the dynamics of wetting layer enrichment for binary mixture and the evolution of SDSD waves have a tight relation with the phase behavior of the cross-sections parallel to substrate surface.

To gain insight into the mechanism, thus, we numerically simulate the substrate-directed spinodal decomposition in 3D by CDS in this study. The Cahn–Hilliard–Cook (CHC) equation was used to investigate the substrate-directed spinodal decomposition in 3D. The frame of this paper is as follows: the models and algorithm are introduced inSection 2. Section 3 presents the simulation results and discussions. Finally, the conclusions are drawn in Section 4.

2. Models and algorithm

Here the dynamics and morphology evolution are described, in the spirit of linear irreversible thermodynamics, by the CHC equation for diffusive field, which can be written as [40]

$$\frac{\partial\psi(r,t)}{\partial t} = M\nabla^2\frac{\delta F(\psi(r,t))}{\delta\Psi(r,t)} + \eta(r,t) \tag{1}$$

Here $\psi(r,t)=\phi(A)-\phi(B)$ is the order parameter of the system at point r at time t. $\phi(A)$ and $\phi(B)$ are, respectively, the local volume fraction of A and B components. We have used the fact that $\psi(r,t)$ is a conserved order parameter. M is a phenomenological parameter. $F(\psi(r,t))$ is usually the coarse-grained free-energy function. In the present study, we chosen z-axis as the direction of the surface effect and consider a substrate surface located at $z=1$. Thus, for the surface-directed spinodal decomposition, $F(\psi(r,t))$ can be defined as [32]

$$\frac{F(\psi(r,t))}{k_BT} = \int \mathrm{d}r\left[\frac{\varepsilon}{2}\psi(r,t)^2 + \frac{u}{4}\psi(r,t)^4 + \frac{c}{2}(\nabla\psi(r,t))^2 - \sum_n \frac{1}{n}[S^{(n)}(z)]\psi(r,t)^n\right] \tag{2}$$

where $S(z)$ describes the surface fields and T is the temperature. ε, u and c are phenomena parameters and can be related to the molecular characteristic [41]. $n=1$ is set in the simulation that indicates an integrated substrate potential [32,51]. And $\eta(r,t)$ is a Gaussian white noise, representing the thermal fluctuation, with mean zero and correlation

$$\langle\eta(r,t)\eta(r',t)\rangle = -2k_BTM\nabla^2\delta(r-r')\delta(t-t') \tag{3}$$

where T is the temperature of the fluid and $\langle\ldots\rangle$ denotes the ensemble average. As a minimal model, any hydrodynamics effects and possible nonlocality in the mobility coefficient can be ignored [42,43]. For simplicity, the thermal noise is also neglected in this simulation. But we must point out that the thermal noise has an effect on the final phase morphology to a certain extent. The effect of noise will be discussed in the other work. The driving force of the phase separation is due to the chemical potential $\mu(r,t)$ with $\mu(r,t)=\delta F(\psi(r,t))/\delta\psi(r,t)$. According to Eq. (2), the chemical potential has the form

$$\frac{\mu(r,t)}{k_BT} = \varepsilon\psi(r,t) + u\psi(r,t)^3 - c\nabla^2\psi(r,t) - \sum_n S^{(n)}(z)\psi^{n-1} \tag{4}$$

with the substitution of the dimensionless variables

$$r\to\frac{r}{\sqrt{\frac{c}{\varepsilon}}},\quad \tau\to\frac{t}{\left(\frac{c}{M\varepsilon^2k_BT}\right)},\quad \psi(r,\tau)\to\frac{\psi(r,t)}{\sqrt{\frac{\varepsilon}{u}}} \tag{5}$$

Then, Eq. (2) becomes

$$\frac{\partial\psi(r,\tau)}{\partial t} = \nabla^2\left[\psi+\psi^3-\nabla^2\psi-\sum_n S^{(n)}(z)\psi^{n-1}\right] \tag{6}$$

The boundary conditions at the substrate can be defined as

$$\nabla\mu(r,\tau) = 0|_{Z=1} \tag{7}$$

$$\nabla\psi + \sum_n S^{(n)}\psi^{n-1} = 0|_{Z=1}$$

Eq. (4) is numerically solved by using the cell dynamics (CDS) proposed by Puri and Oono [44,45]. In the 3D CDS, the system is discretized on a $L_a\times L_a\times L_a$ cubic lattice. And the order parameter of each cell is defined as $\psi(r,\tau)$, where

$r=(r_x,r_y,r_z)$ is the lattice position and r_x, r_y, and r_z are integers between 1 and L_a. According to CDS, the polynomial $\psi+\psi^3-\nabla^2\psi$ is replaced by $A\tanh\psi-\psi+D[\langle\langle\psi\rangle\rangle-\psi]$, where A is a phenomenological parameter characterizing the quenching depth and D can be related to the interfacial free energy. And $\langle\langle\psi(r)\rangle\rangle$ represents the following summation of $\psi(r)$ for the nearest neighbors (*r.*), the next-nearest neighbors (*r.r.*), and the next-next-nearest neighbors (*r.r.r.*)

$$\langle\langle\psi(r)\rangle\rangle = B_1\sum_{r=r.}\psi(r)+B_2\sum_{r=r.r.}\psi(r)+B_3\sum_{r=r.r.r.}\psi(r) \quad (8)$$

where B_1, B_2, and B_3 are 6/80, 3/80 and 1/80 for the 3D system. Considering only the long-range potential, the surface effect can be transformed into $H_a(1+(Z-1)^3)^{-1}$, where H_a is of order the total integrated surface potential [32]. Then, Eq. (6) is transformed to the following difference equation:

$$\psi(r,\tau+1)=\psi(r,\tau)-R(\langle\langle I(r,\tau)\rangle\rangle-I(r,\tau)) \quad (9)$$

with

$$I(r,\tau)=A\tanh\psi-\psi+D[\langle\langle\psi\rangle\rangle-\psi]+\frac{H_a}{1+(Z-1)^3} \quad (10)$$

Discretizing the boundary conditions, i.e. Eq. (7), at substrate surface ($z=1$) gives $\psi(-1,\tau)=\psi(1,\tau)$ and $I(-1,\tau)=I(1,\tau)$. Furthermore, the periodic boundary conditions are used in the x and y directions and free boundary conditions are applied at the other end in the z direction.

The parameters are set $A=1.3$, $D=0.7$, and $R=1$ in the present simulation, respectively. The surface interaction parameter H_a is set $H_a=0.15$. Our simulation was carried out on $L_a\times L_a\times L_a=64\times64\times64$ 3D cubic lattice. And the dimensionless spatial increment is $\Delta x=\Delta y=\Delta z=1$. The dimensionless time step is set as $\Delta\tau=1$. The range of the field ψ at $\tau=0$ is $\bar{\psi}-s\le\psi\le\bar{\psi}+s$ with the random fluctuation $s=0.1$, where the spatial average of ψ is $\bar{\psi}=0$. The initial conditions correspond to the case of critical quenches.

3. Results and discussions

3.1. Time evolution of simulated patterns

First we show how SDSD processes in three dimensions. Fig. 1 indicates the pattern evolution of SDSD. In Fig. 1, regions with positive order parameter (*A* rich phase; say, *A*—rich) are marked with the color bar and those with a negative order parameter (*B* rich phase; say, *B*—rich) are pure black. It can be clearly seen from Fig. 1 that the wetting surface layer rapidly changes and becomes an *A*—rich cross-section, followed by *B*—rich cross-section. The longer the time, the thicker the *A*—rich cross-section is.

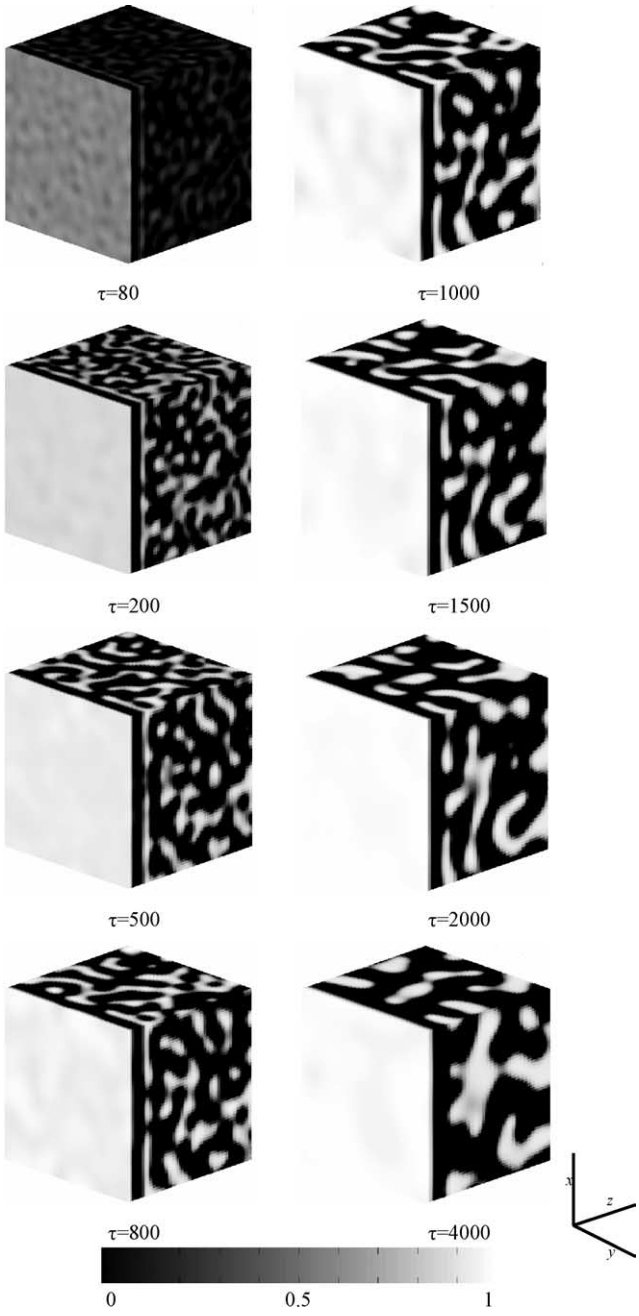

Fig. 1. Simulated pattern evolution of surface-directed spinodal decomposition in 3D with $H_a=0.15$. The color bar denotes the magnitude of the positive order parameters.

Next to the *B*—rich cross-section, one can see a very clear two-phase structure showing a typical percolated network patterns before $\tau=800$. However, after $\tau=800$, it can be found the break up of the percolated network. The percolated network gradually disrupts or breaks up into many fragments. With further increasing time, the irregularly shaped fragments shrink and then reshape into many anisotropic drops and droplets. The simulation reproduces the basic features of experimental observation [3–10].

Some cross-sections parallel to the substrate surface,

which have not been investigated until the present study, can be taken out to study the evolution of the phase morphology along z-axis. Fig. 2 shows that the phase morphologies at different locations along z-axis at $\tau=500$. The patterns are almost pure white at $z=2$ and almost pure black at $z=6$, demonstrating the A—rich cross-section and B—rich cross-section, respectively. Along the z-axis, the A component increases gradually and reach a maximum. It is interesting that a sudden phase inversion appears after $z=10$. The A phase is dispersed in B continuous phase with droplets. With further increasing z value, the size of A phase increases gradually and turns to percolated network again. Thus, the morphology in order of the increasing z is as follows: (a) an A—rich cross-section at the substrate surface, (b) a B—rich cross-section, (c) A droplet morphology with A as the majority phase, and (d) a bicontinuous morphology associated with spinodal decomposition in the bulk. The phase inversion can be observed clearly in 3D simulations by investigation of the phase morphology of the cross-section parallel to the substrate.

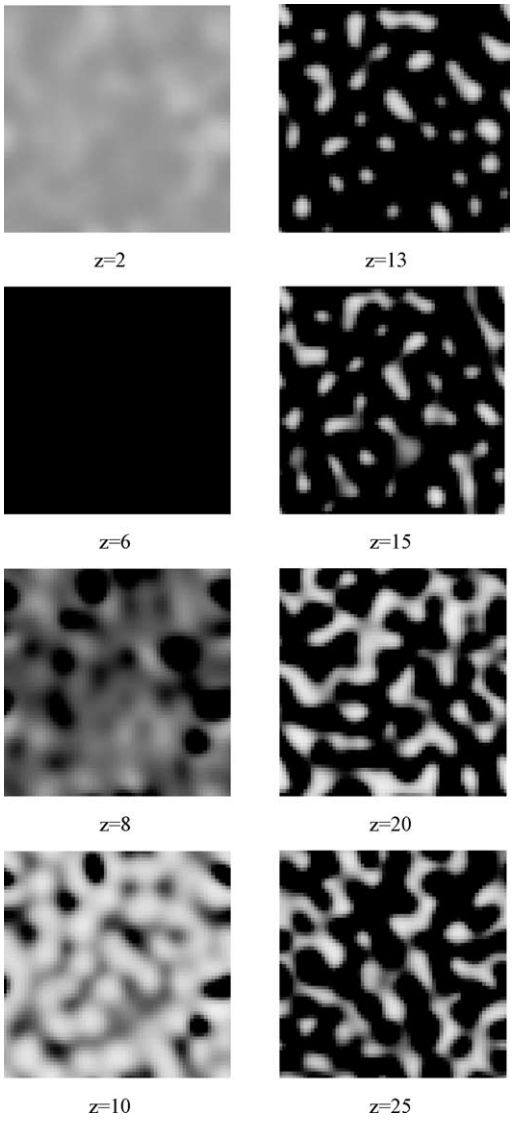

Fig. 2. Simulated pattern evolution at different values of z with $\tau=500$.

3.2. Analysis for the cross-sections parallel to the substrate

3.2.1. Evolution of the wetting layer

Fig. 3(a) shows the averaged profiles in the z direction for the evolution of the patterns of Fig. 1. The averaged profiles are obtained by averaging the order parameter profile $\psi(x,y,z,\tau)$ of the cross-sections along z-axis as Eq. (11) with $N_{x,y}=\psi_{\mathrm{av}}(0,\tau)$ for a single run and then ensemble averaging over 50 different runs. Fig. 3(b) shows some average profiles within smaller values of z.

$$\psi_{\mathrm{av}}(z,\tau)=\frac{1}{N_{x,y}}\sum_{x,y}\psi(x,y,z,\tau) \tag{11}$$

It is seen that the hallmark of substrate-directed spinodal decomposition, i.e. a profile that oscillates with a

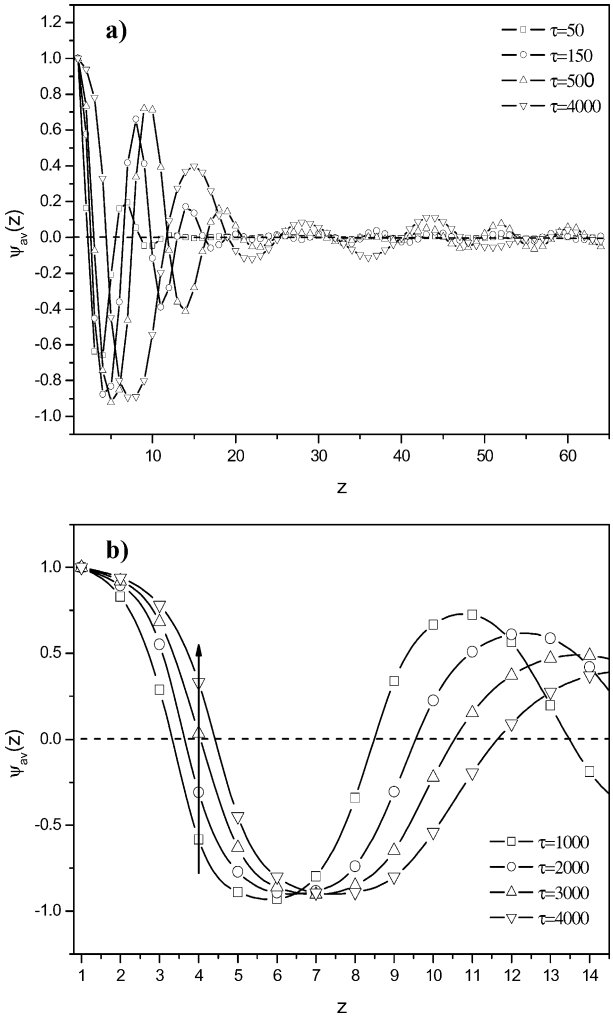

Fig. 3. The averaged profiles in the z direction for the patterns in Fig. 1 at different times: (a) within full scale of z (b) within shorter rang of z near the substrate surface. The arrow in (b) indicates the evolution of the order parameter at $z=4$.

characteristic wavelength, is presented near the substrate surface, which slowly propagates out into the bulk. And the averaged profiles decay to zero in the bulk where spinodal decomposition waves are isotropic and randomly oriented.

The thickness of the surface layer can be measured by finding the z position $R(\tau)$ of the first zero of the z-order parameter profile. Fig. 4(a) shows the evolution of $R(\tau)$ with the increasing time, τ. It is obvious that the growth of this surface layer is extremely faster in the early stage. In the log–log scale (Fig. 4(b)), the evolution of $R(\tau)$ presents approximately a line with slope to be about 1/8, corresponding to the result of Puri [28]. For the case with conserved order parameter and lower potential, Lipowsky [46] predicted exponent twice as large, i.e. 1/4. Our results demonstrate that the LS growth law cannot be used to characterize the growth of the wetting layer in this case. And the growth law of the surface layer is really a surface-potential-dependent growth law [29,30].

It should be noted that the growth mechanism of the surface layer has an important correlation with H_a. And different values of H_a can lead to different growth laws of the surface layer such as surface-potential-dependent, Lifshitz–Slyozov (LS), interface diffusive and logarithmic growth laws [2,52]. The simulated results of the relationship between the surface interaction and the wetting layer will be discussed in detail in the next paper [52].

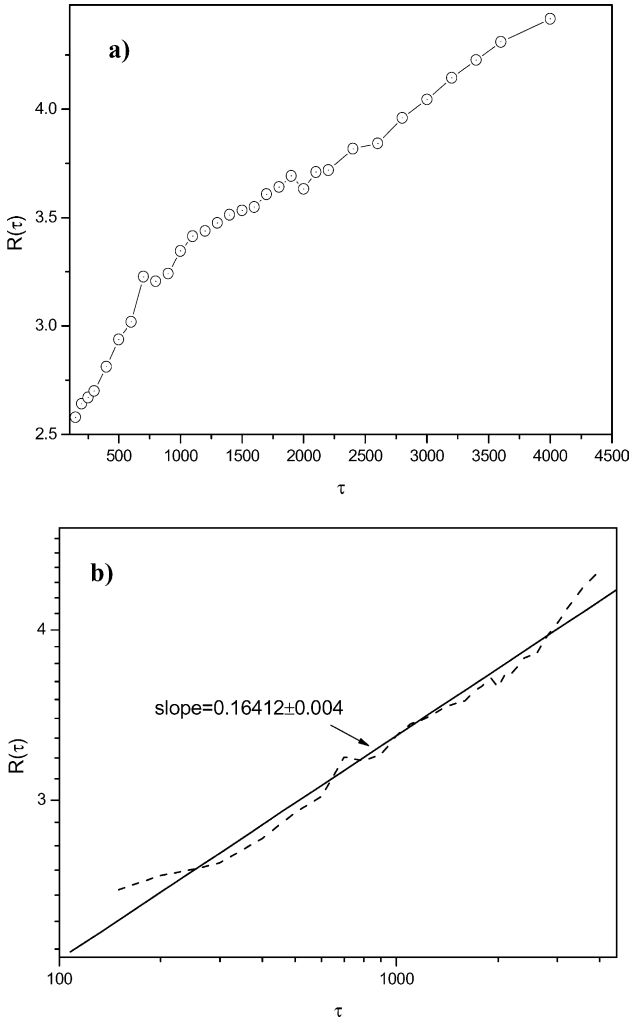

Fig. 4. (a) The plot of $R(\tau)$ with the increasing time,τ. (b) The plot of (a) in the log–log scale.

3.2.2. Formation mechanism of the wetting surface layer

Some researches have investigated the formation mechanism of wetting surface layer in both diffusive and hydrodynamic cases [32,47]. The enrichment of wetting surface layer is difficult to study experimentally. However, using 3D simulation, it can be analyzed conveniently by investigating the phase evolution of the parallel cross-sections near the substrate surface.

To understand how the wetting surface layer forms, the formation of the spreading surface domains on the cross-section at $z=4$, which is near the substrate surface, is investigated. From Fig. 3(b), one can find that the cross-section at $z=4$ is located in B—rich domain at the initial stage. Then, with the increasing time, the averaged order parameter at $z=4$ grows up and changes into A—rich cross-section gradually. This procedure indicates the formation of the spreading surface domain of the wetting layer near the substrate. Fig. 5 shows the morphology evolution of the cross-section at $z=4$. It can be clearly seen that the cross-section in the early and interim stages is almost pure black, implying that the cross-section is located in the B—rich domain at those times. Then, a particle of A component appears as pointed by the arrow. The particle becomes bigger with the increasing time while some other particles also come forth randomly. These particles connect to each other and coarsen gradually. Then, A component occupies almost the whole surface in the late stage. Fig. 6 is the schematic diagram for the enrichment of the wetting surface layer in side view. The model used in the present study is model B which only describes the diffusive effect [48]. The simulated results demonstrate that it is the continuous influence of anisotropic diffusive behavior arose by the attraction of the substrate that incorporates the random bulk domain into spreading surface domains of the wetting layer on the substrate. Then, the small droplets of the wetting phase coarsen into a much larger one.

3.2.3. Concentration fluctuation near substrate surface

Fig. 7 shows the morphology evolution of the surface at $z=4$. There are many particles of A component dispersed in continuous phase of B component in the early stage. With the increasing time, the growth of these particles leads to the connection of A component and turns into the typical percolated phase structure. Then, it can be found that almost only A component is in the pattern at $\tau=500$. With the further increasing time, many holes are presented in the pattern. And these holes become bigger and bigger, which corresponds to the spreading of the surface domains of the substrate in contact with the random bulk domains.

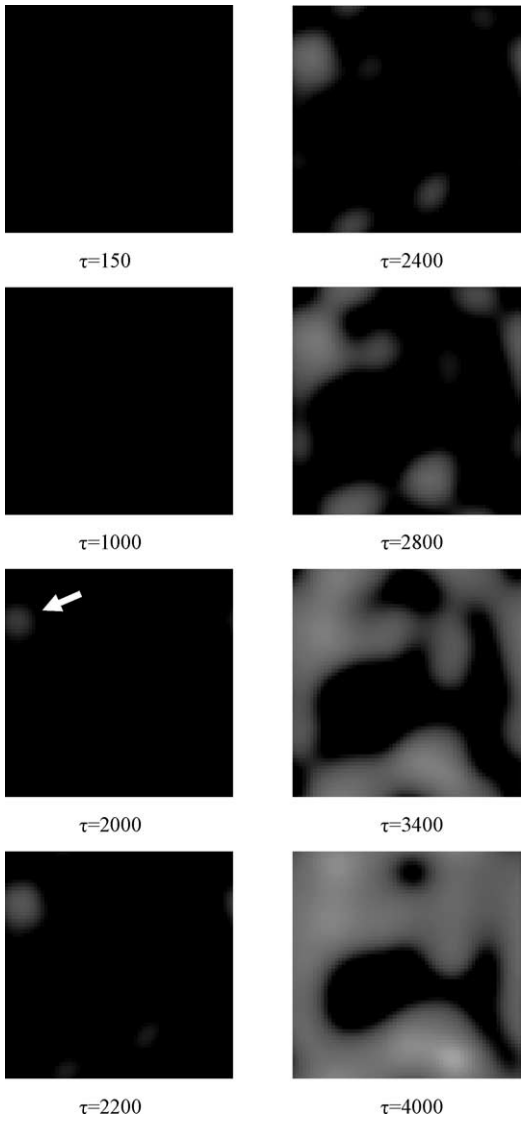

Fig. 5. Simulated patterns at with $z=4$ different times. The arrow at $\tau=2000$ points out the initial formation of the A component particle.

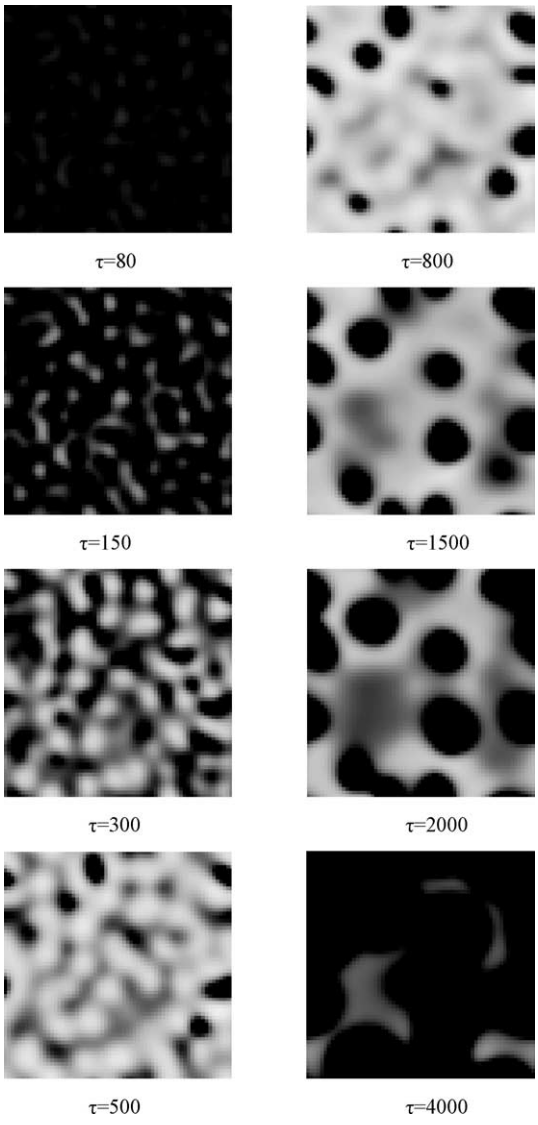

Fig. 7. Simulated patterns at different times with $z=10$.

A component decreases gradually with the percolation of phase structure. Thus, the concentration at the cross-section near the substrate interface fluctuates with the increasing time. It is interesting that the phase inversion happens at about $\tau=500$.

Fig. 8 shows the plots of z-order parameter at different times. These plots show that the concentration waves shift further to large values of z with the increasing time. It is seen that the points, at the line $z=10$, move from the right side of the first peak to the left with the increasing time, and get to the wave peak at about $\tau=500$. Corresponding to Fig. 7, it can be found that the concentration fluctuates near the first wave peak and, the inversion of the phase morphology happens at the wave peak. The phase morphologies of the two sides of the first wave are different completely. And one is the typical percolated phase structure; the other is the continuous phase of A component with many holes of B component due to the attraction force of the substrate.

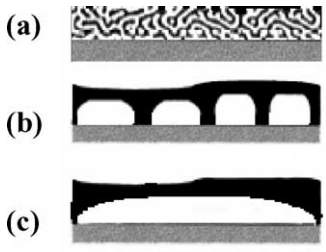

Fig. 6. The schematic diagram for the enrichment of the wetting surface layer in side view. (a) Early stage (b) Interim stage (c) Late stage.

To more clearly understand the concentration fluctuation near substrate interface, the evolution of average characteristic length near substrate interface is also analyzed. To do so, the characteristic length, Λ, and its average, Λ_m, of certain cross-sections at different times are calculated as follow [16]

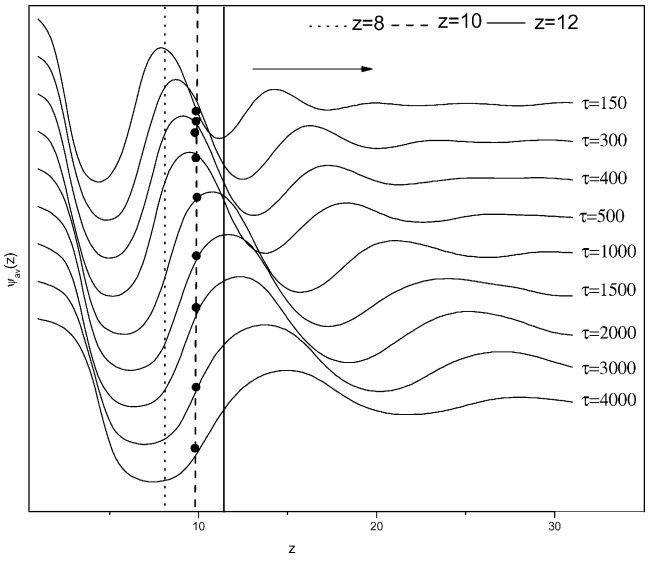

Fig. 8. Plots of averaged order parameter profile against z at different times. The arrow indicates that the profiles shift into the bulk with the increasing time.

$$\Lambda m = \int_0^{+\infty} \Lambda P(\Lambda) \mathrm{d}\Lambda \tag{12}$$

with

$$P(\Lambda) = \frac{N(\Lambda)}{\int_0^{+\infty} N(\Lambda)\mathrm{d}\Lambda} \tag{13}$$

where $N(\Lambda)$ is a frequency of the events Λ. Fig. 9 shows the temporal changes of Λ_m at different values of z. The growth of Λ_m at $z=10$ is fast in the early stage. Then, a clear wave peak appears at about $\tau=500$. With further increasing time, Λ_m decreases, reflecting the inversion of the average size of the phase at about $\tau=500$. At the same time, it is clear seen that the peak of inversion appears in more early stage at $z=8$, then, the characteristic length decreases quickly.

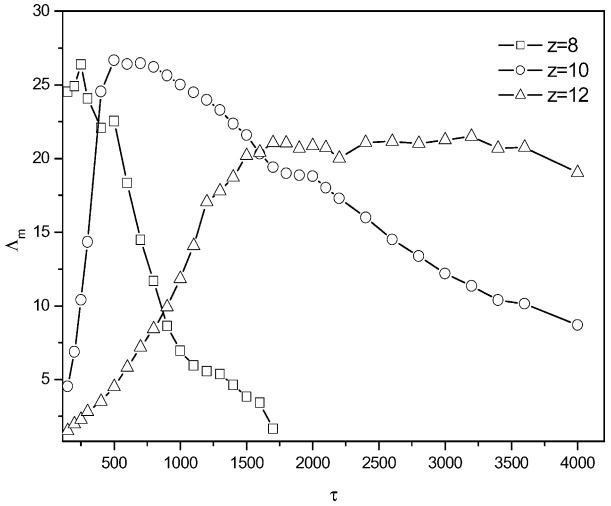

Fig. 9. The temporal changes of Λ_m at different values of z.

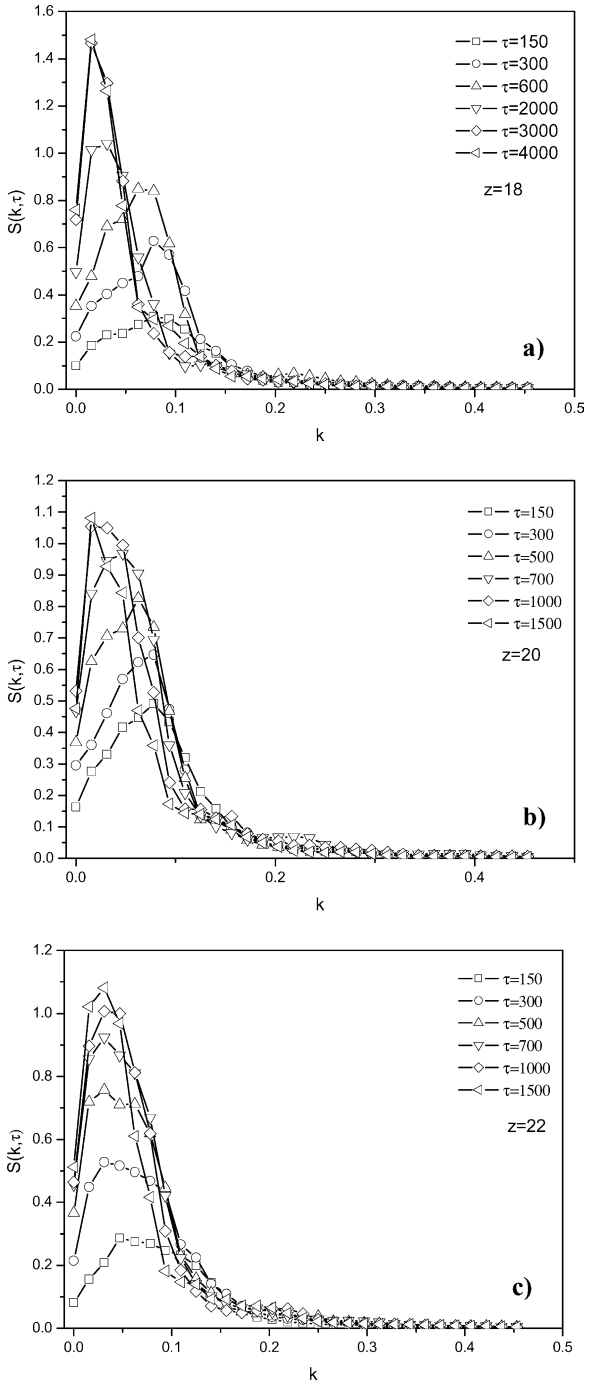

Fig. 10. Plots of $S(k,\tau)$ against k at different times for three values of z.

At $z=12$, the change of Λ_m becomes bigger in the early stage, but no peak is presented in the curve. These results are consistent with that of Fig. 8. It is clear seen that the intersection points between the line of $z=8$ and plots of $\psi_{av}(z)$ are almost only located at the unilateral side of the peak and, move from wave peak to valley. To the contrary, the intersection points of $z=12$ move from wave valley to the peak of the first peak. Only for $z=10$ the intersection points move from the right side of the first peak to the left side with the increasing time. Thus, it can be seen that the

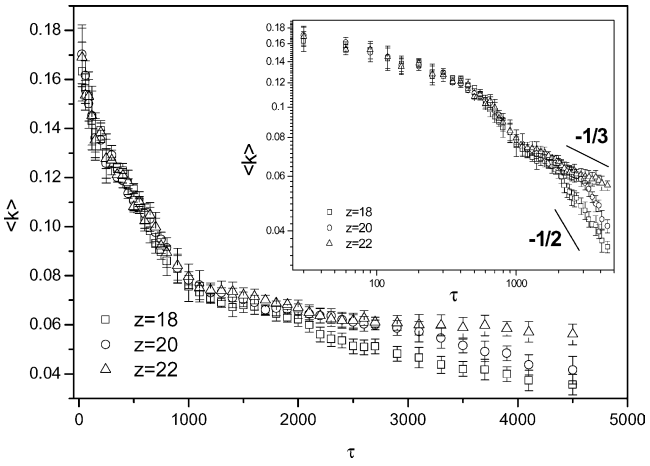

Fig. 11. Plots of $\langle k \rangle$ against time τ for $z = 18, 20, 22$. The inset is the plots in the log–log scale.

evolutions of the phase morphology and average size near the surface layer fluctuate greatly due to the attraction of the substrate.

3.2.4. Dynamical evolution of the parallel cross-sections

Fig. 10 shows the time evolution of the scattering function $S(k,\tau)$ for different z values ($z = 18$, 22, 24). It is clear that with the increasing time, the scattering intensity becomes higher and, the maximum of the intensity shifts to smaller wavenumber. The time evolution of the scattering function, $S(k,\tau)$, is in a normal mode for phase separation at different locations. In this section, we define the characteristic length scale of the pattern size based on $S(k,\tau)$. And the characteristic length $\langle k \rangle$ is defined as

$$\langle k \rangle = \frac{\int k S(k,\tau) \mathrm{d}k}{\int S(k,\tau) \mathrm{d}k} \tag{14}$$

Fig. 11 shows plot of $\langle k \rangle$ against time τ for $z = 18, 20, 22$. All results are averaged over fifty independent runs. It is found that the plots can be superposed in the early stage. However, these plots cross over at different times in the late stage, respectively. On the other hand, the length-scale data for different values of z evolves with almost the same speed initially and then cross over to a faster growth as the effect of the substrate is transported and inducted. The crossover is later for larger values of z. The inset clarifies the crossover. Before the crossover, the growth law is $\langle k \rangle \propto \tau^{-1/3}$, demonstrating the typical LS growth law. Subsequent to the crossover, the accelerate growth seems to fit a faster law with about $\langle k \rangle \propto \tau^{-1/2}$. The data in the crossover regime may be associated with the orientation effect due to the spreading of the preferred component on substrate. In this case, a part of interconnected structure of polymer mixture could be broken up and result in extended strands parallel to the substrate surface. Thus, the phase structure near the wetting layer on the substrate coarsens due to interfacial diffusion at

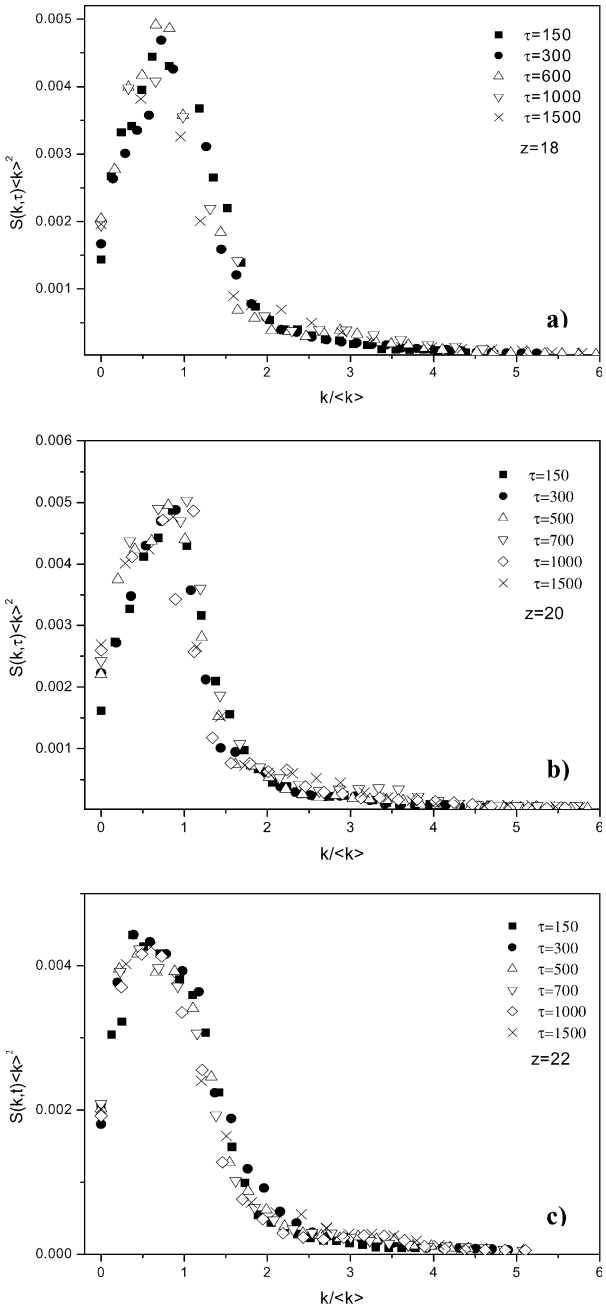

Fig. 12. Plots of the scale law function $S(k,\tau)\langle k \rangle^2$ against $k/\langle k \rangle$ at different times for three different values of z.

the crossover time, which follows a $\tau^{-1/2}$mechanism [5,49,50]. Fig. 12 shows the superposed data from different times for the scale law function $S(k,\tau)\langle k \rangle^2$ versus $k/\langle k \rangle$ for three different values of z. These plots fall on a master curve with the increasing time, respectively, demonstrating the self-similar evolution of the phase in each cross-section.

3.3. Analysis for the cross-sections perpendicular to the substrate

3.3.1. Phase evolution of the perpendicular cross-section

To more clearly understand the phase evolution of the

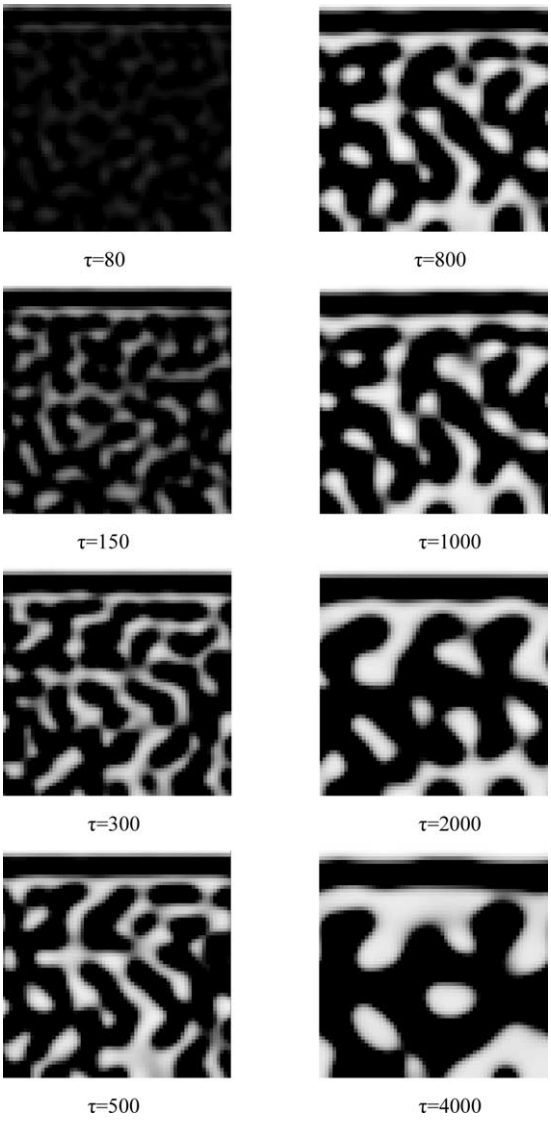

Fig. 13. Simulated patterns with $x=32$ at different times.

cross-section perpendicular to the substrate, the cross-section in x direction with $x=32$ is investigated. Fig. 13 shows the evolution of the cross-sections at different times. Along the z-axis and from the substrate, the wetting layer of A component parallel to the substrate rapidly forms on the substrate followed by a cross-section of B component. The next is another enriched cross-section of A component, which has about the same average thickness as the wetting layer adjacent to the substrate. Moreover the domain pattern farther from the substrate has just the characteristic structure of bulk spinodal decomposition. The dynamics of the phase separation in the vicinity of the substrate is enhanced due to the orientation effect of the substrate that preferentially aligns domains parallel to it. These result in anisotropy of domain growth parallel and perpendicular to the surface, in the vicinity of the substrate. The extent of the anisotropy decreases with increasing z value and, the bulk is isotropic. These results correspond to that of the analysis by 3D.

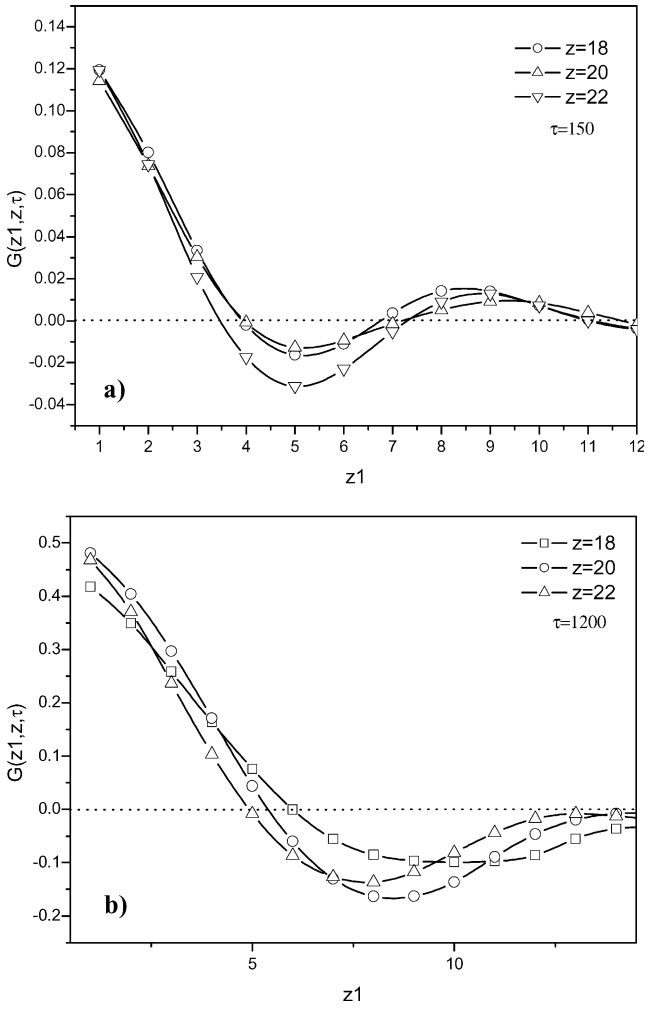

Fig. 14. Data for the surface averaged correlation function $G(z1,z,\tau)$ as a function of $z1$ at different times (a) $\tau=150$ (b) $\tau=1200$.

3.3.2. Dynamical evolution of the perpendicular cross-sections

We next consider the scaling behavior of real-space correlation functions, which are used in characterizing the dynamics of fluctuations. z-Dependent correlation function perpendicular to the substrate can be defined as [27,28]

$$G(z1,z,\tau)=\langle\psi(x,y,z,\tau)\psi(x,y,z+z1,\tau)\rangle - \langle\psi(x,y,z,\tau)\rangle\times\langle\psi(x,y,z+z1,\tau)\rangle \quad (15)$$

The angular brackets refer to an averaging over initial conditions and integration over x and y.

Furthermore, the characteristic length in the perpendicular direction, L, can be defined as

$$G(z+L,z,\tau)=\frac{G(0,z,\tau)}{2} \quad (16)$$

where $G(0,z,\tau)$ is the maximum value of $G(z1,z,\tau)$.

Fig. 14(a) and (b) show data for the surface averaged correlation function $G(z1,z,\tau)$ as a function of $z1$ from early to later stage. Because of the breaking of translational

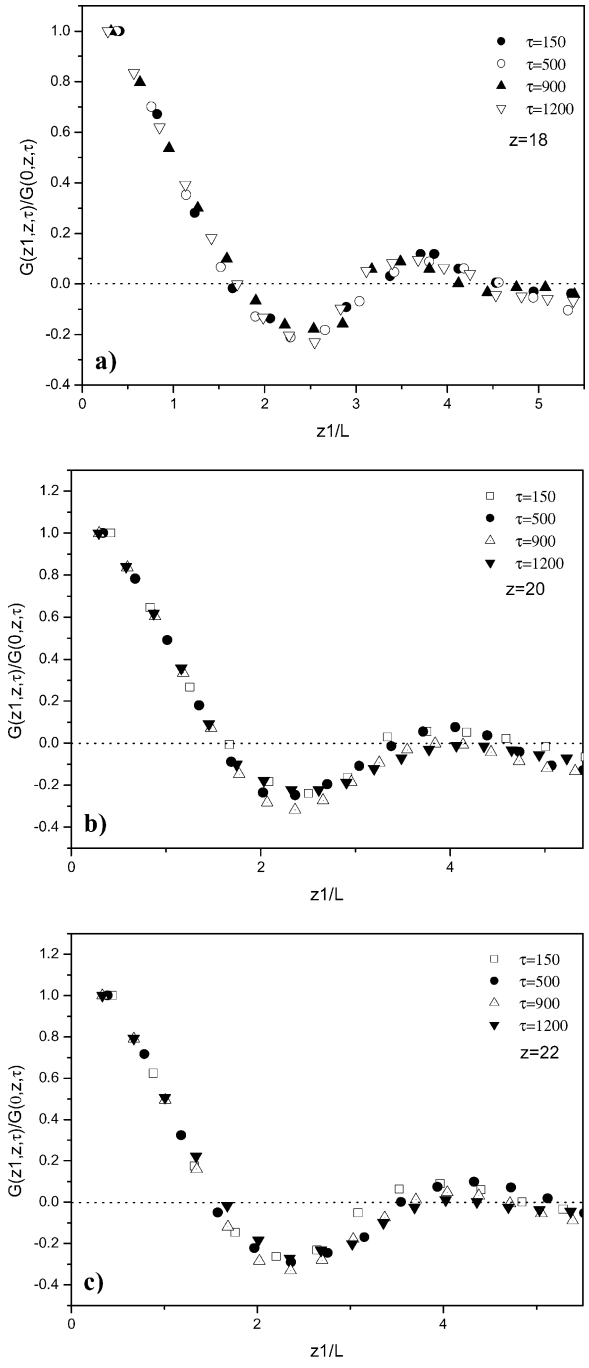

Fig. 15. Plots of the normalized correlation function $G(z1,z,\tau)/G(0,z,\tau)$ against $z1/L$ at different times for three values of z.

symmetry by the substrate, the correlation function depends on both z and $z1$, until one is deep into the bulk. Fig. 15(a)–(c) give plots of the normalized correlation function $G(z1,z,\tau)/G(0,z,\tau)$ against $z1/L$ at different values of z at different times. It is obvious that the correlation functions exhibit reasonable scaling, implying the self-similar dynamical evolution of the phase morphology in the perpendicular cross-section. We must point out that the scale law in the perpendicular cross-section is only obtained in the short distance of $z1$, i.e. within the first wavelength of $z1/L$.

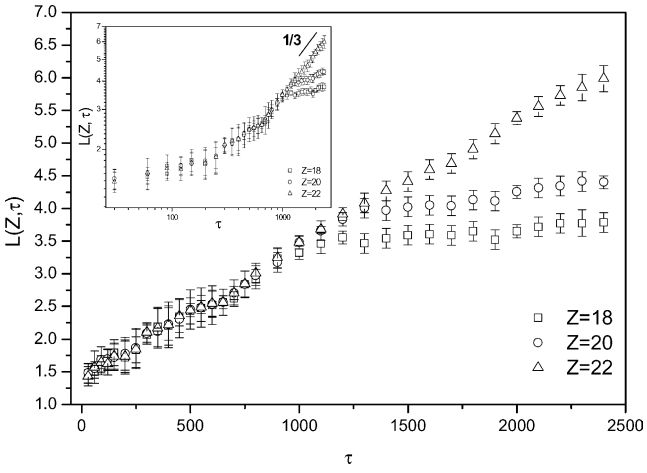

Fig. 16. Plots of $L(z,\tau)$ against τ for $z=18$, 20, 22. The inset is the plots in log–log scale.

Fig. 16 shows plots of $L(z,\tau)$ against τ for $z=18$, 20, 22. And the inset is the plots in log–log scale. All results are averaged over 50 independent runs. Correlated with Fig. 11, it is seen that both the perpendicular and parallel length scales follow the LS growth law until they experience the effect of the wetting layer. In the late stage, the perpendicular length scale exhibits decelerated growth and even freezes at longer time. The freezing does not mean that there is no temporal evolution, but a dynamical equilibrium process. The cross-section at z is not located in the region of bicontinuous morphology, but in the region of the droplet because of the depletion of A component by the substrate effect, whereas $z1$ still locates in the region of bicontinuous morphology.

4. Conclusions

The simulated morphologies and evolutions of the substrate effect spinodal decomposition are basically consistent with what was observed in experiments. It is found that the phase inversion happens at the parallel cross-section near the substrate interface. The simulation indicates that the variation rule of the average character length at the cross-section near the substrate corresponds to that of the average order parameter. And a phase inversion is observed at about the peak of the first wave.

The increase of the wetting layer thickness presents approximately a line with slope being about 1/8, demonstrating that the Lifshitz–Slyozov (LS) growth law cannot be used for the growth of the wetting layer. The simulation indicates that the continuous influence of anisotropic diffusive behavior arose by wetting of substrate induces the wetting component spreading onto the interface of the substrate randomly.

The phase evolution, on the cross-sections both perpendicular and parallel to the substrate, follows the LS growth law until they experience the effect of the wetting

layer. And the parallel length scale shows accelerated growth with $\tau^{1/2}$, while the perpendicular scale exhibits decelerated growth and can even freeze. And the results obtained by scale function $S(k,\tau)\langle k\rangle^2$ against $k/\langle k\rangle$ demonstrate the self-similar evolution of the phase in each parallel cross-section. The data of the averaged correlation function $G(z1,z,\tau)$ indicates the self-similar dynamical evolution of the phase morphology in the perpendicular cross-section within about one wavelength distance of $z1/L$.

Acknowledgements

Financial support from the National Natural Science Foundation of China (No.90103035, No.20174022 and No.10334020) and the Specialized Research Fund for the Doctoral Program of Higher Education (No.20040003033) is highly appreciated.

References

[1] Puri S. J Phys Condens Matter 2005;17:R101–R42 [and references therein].
[2] Geoghegan M, Krausch G. Prog Polym Sci 2003;28:261–302 [and references therein].
[3] Jones RAL, Norton LJ, Kramer EJ, Bates FS, Wiltzius P. Phys Rev Lett 1991;66:1326–9.
[4] Krausch G, Dai C-A, Kramer EJ, Bates FS. Phys Rev Lett 1993;71: 3669–72.
[5] Wang W, Shiwaku T, Hashimoto T. Macromolecules 2003;36: 8088–96.
[6] Xie X-M, Xiao T-J, Zhang Z-M. J Colloid Interface Sci 1998;206: 189–94.
[7] Xie X-M, Kong X-M, Xiao T-J, Yang Y, Gao N, Tanioka A. J Colloid Interface Sci 2001;234:24–7.
[8] Xie X-M, Chen Y, Zhang Z-M, Tanioka A, Matsuoka M, Takemura K. Macromolecules 1999;32:4424–9.
[9] Zong Q, Li Z, Xie X-M. Macromol Chem Phys 2004;205:1116–24.
[10] Liu YD, Kong X-M, Xie X-M. Acta Polym Sin 2002;(6):824–7.
[11] Brown G, Chakrabarti A, Marko JF. Phys Rev E 1994;50:1674.
[12] Straub W, Bruder F, Brenn R, Krausch G, Bielefeldtm H, Krisch A, et al. Europhys Lett 1995;29:353–61.
[13] Wiltzius P, Cumming A. Phys Rev Lett 1991;66:3000–3.
[14] Cumming A, Wiltzius P, Bates FS, Rosedale JH. Phys Rev A 1992;45: 885–97.
[15] Guenoun P, Beysens D, Robert M. Physica A 1991;172:137–40.
[16] Nakai A, Shiwaku T, Wang W, Hasegawa H, Hashimoto T. Macromolecules 1996;29:5990–6001.
[17] Sung L, Karim A, Douglas JF, Han CC. Phys Rev Lett 1996;76: 4368–71.
[18] Geoghegan M, Jones RAL, Clough AS. J Chem Phys 1995;103: 2719–24.
[19] Geoghegan M, Ermer H, Jüngst G, Krausch G, Brenn R. Phys Rev E 2000;62:940–50.
[20] Karim A, Douglas JF, Lee BP, Glotzer SC, Rogers JA, Jackman RJ, et al. Phys Rev E 1998;57:R6273–R6.
[21] Böltau M, Walheim S, Mlynek J, Krausch G, Steiner U. Nature 1998; 391:877–9.
[22] Kargupta K, Sharma A. Phys Rev Lett 2001;86:4536–9.
[23] Kargupta K, Sharma A. Langmuir 2002;18:1893–903.
[24] Ginzburg VV, Qiu F, Balazs AC. Polymer 2002;43:461–6.
[25] Patnaik SS, Pachter R. Polymer 2002;43:415–24.
[26] Feng J, Ruckenstein E. Polymer 2002;43:5775–90.
[27] Puri S, Binder K. Phys Rev E 1994;49:5359–77.
[28] Puri S, Binder K. Phys Rev E 1997;56:6991–7000.
[29] Puri S, Binder K. Phys Rev Lett 2001;86:1797–800.
[30] Puri S, Binder K. Phys Rev E 2002;66:061602.
[31] Lee BP, Douglas JF, Glotzer SC. Phys Rev E 1999;60:5812–22.
[32] Marko JF. Phys Rev E 1993;48:2861–79.
[33] Kuksenok O, Balazs AC. Phys Rev E 2003;68:011502.
[34] Binder K, Frisch HL. Physica B 1991;84:403–9.
[35] Sagui C, Somoza AM, Roland C, Desai RC. J Phys A Math Gen 1993; 26:L1163–L8.
[36] Rysz J. Polymer 2005;46:977–82.
[37] Puri S, Binder K. Phys Rev A 1992;46:R4487–R9.
[38] Gestoso P, Brisson J. Polymer 2003;44:7765–76.
[39] Lam Y-M, Goldbeck-Wood G. Polymer 2003;44:3593–605.
[40] Gunton JD, San Miguel M, Sahni PS. In: Domb C, Lebowitz J, editors. Phase transitions and critical phenomena. London: Academic Press; 1990.
[41] Ohata T, Enomoto Y, Harden JL, Doi M. Macromolecules 1993;26: 4928–34.
[42] Luo K, Yang Y. Macromolecules 2002;35:3722–30.
[43] Luo K, Yang Y. Polymer 2004;45:6745–51.
[44] Oono Y, Puri S. Phys Rev A 1988;38:434–53.
[45] Puri S, Oono Y. Phys Rev A 1988;38:1542–65.
[46] Lipowsky R. J Phys A 1985;18:L585–L90.
[47] Frisch HL, Puri S, Nielaba P. J Chem Phys 1999;110:10514–21.
[48] Onuki A. Phase transition dynamics. London: Cambridge University Press; 2002.
[49] San Miguel M, Grant M, Gunton JD. Phys Rev A 1985;31:1001–5.
[50] Grant M, Elder KR. Phys Rev Lett 1999;82:14–16.
[51] de Gennes PG. Rev Mod Phys 1985;57:827–63.
[52] Yan L-T, Xie X-M. Submitted to Polymer.